IOP Publishing Journal of Physics D: Applied Physics
J. Phys. D: Appl. Phys. **53** (2020) 485303 (8pp) https://doi.org/10.1088/1361-6463/abadc3

Current crowding and spreading resistance of electrical contacts with irregular contact edges

Penglu Yang[1], Sneha Banerjee[1], Wenjun Kuang[2], Yu Ding[3], Quan Ma[3] and Peng Zhang[1]

[1] Department of Electrical and Computer Engineering, Michigan State University, East Lansing, Michigan 48824-1226, United States of America
[2] Center for Advancing Materials Performance from the Nanoscale (CAMP-Nano), State Key Laboratory for Mechanical Behavior of Materials, Xi'an Jiaotong University, Xi'an 710049 People's Republic of China
[3] Lam Research, Tualatin, Oregon 97062, United States of America

E-mail: pz@egr.msu.edu

Received 23 June 2020, revised 31 July 2020
Accepted for publication 10 August 2020
Published 4 September 2020

Abstract

Practical electrical contact edges are irregular either macroscopically due to fabrication errors or microscopically due to the nature of edge or surface roughness. However, electrical contact models typically assume ideal and regular contact geometries, where geometrical effects of the irregular electrode edges are not well characterized. This paper studies current crowding and spreading resistance of electrical contacts with irregular contact edges. Using finite element method based numerical simulations, we investigate the scaling of total resistance, spreading resistance, potential drop and current distribution for electrical contacts of tilted contact edges, with various electrode lengths a and edge angles θ. It is found that as the contact edge angle θ increases, the spreading resistance and therefore the total resistance decreases. This is attributed to the increased current crowding towards the corner of the longer electrode side edge when the edge tilt increases, leading to shorter current conduction paths. For a given edge tilt angle θ, the scaling of spreading resistance with a follows closely that of zero edge angle $\theta = 0$: the spreading resistance decreases with a when $a/h < 1$ and then converges to a constant when $a/h > 1$, where h is the thickness of the conductor. The current density distribution near the electrical contacts are shown for different edge angles θ.

Keywords: contact resistance, current crowding, spreading resistance, irregular contact

(Some figures may appear in colour only in the online journal)

1. Introduction

Electrical contacts [1–3] are important to superconducting accelerators [4], high power microwave and millimeter wave sources [5], vacuum switches, and pulsed power systems [6, 7]. They are crucial to the operation of plasma heating systems [8, 9] and high current carrying conductors [10] in International Thermonuclear Experimental Reactor, and Large Hadron Collider [11]. It has been estimated that contact problems account for 40% of all electrical/electronic failures, ranging from small scale consumer electronics to large scale aerospace and military systems [12, 13]. Poor electrical contact prevents efficient power coupling to the load, produces unwanted plasma [14], and even damages system components. On the other hand, electrical contacts and interconnects and their related thermal issues have become one of the most critical concerns in very large scale integration circuit design, due to the excessive heat deposition in the increasingly limited contact space, especially with growing demands for high packing density [15, 16]. For devices based on novel low-dimensional materials, making good electrical contact remains the major challenge, as contact resistance and current

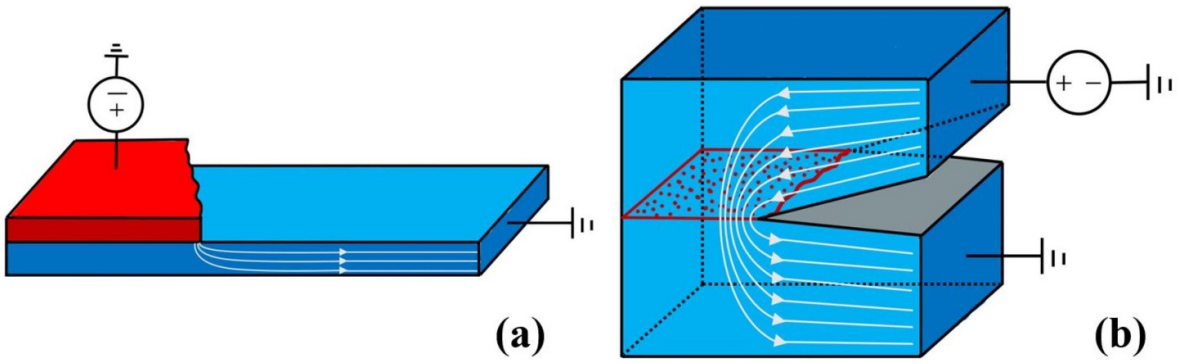

Figure 1. (a) An electrical contact with tilted and/or rough contact edge, and (b) a conducting structure with an irregular shaped crack are given an input bias voltage. The gray lines show the current flow path.

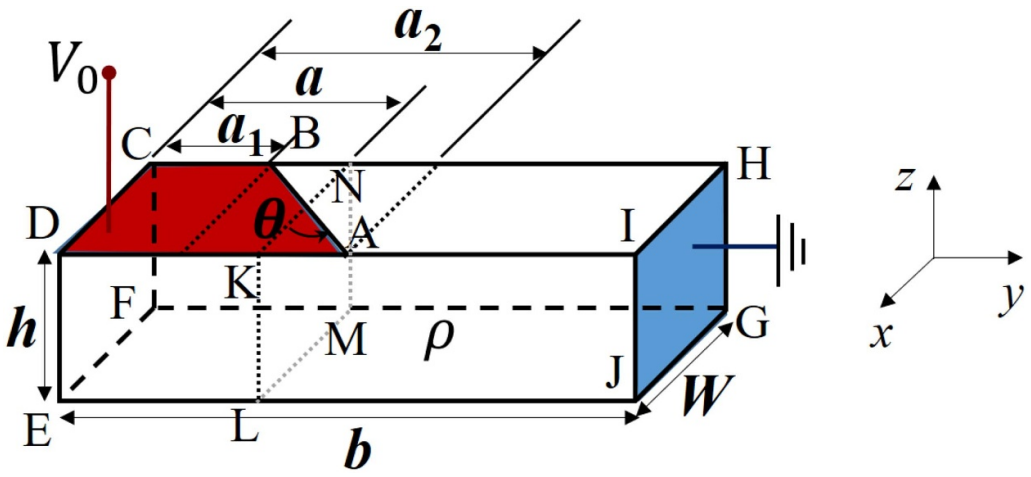

Figure 2. A conducting structure with an electrode contact of tilted edge. Here, a_1 is the length of the shorter side edge of the electrode, and a_2 is the length of the longer side edge. Note that $a = (a_1 + a_2)/2$, and $a_2 - a_1 = W\tan\theta$. The average length of the bulk conductor outside the contact is $L = (L_1 + L_2)/2 = b - a$.

crowding significantly impact and sometimes even dictate the overall device performance [17, 18]. Electrical contacts are also important to micro-electromechanical system (MEMS) [19, 20], semiconductor nanolasers [21, 22], carbon nanofiber based cathodes and field emitters [23–28], and emerging nanoscale vacuum electron devices [29–32].

Electrical contacts are studied mostly by assuming ideal contact geometries [1–3, 33–43]. Examples include circular a-spot, referring to a circular constriction hole at the interface of two current conduction channels [1–3, 34], cylindrical contacts between cylinders or thin film disks of different radii [35, 36, 40], and Cartesian contacts between rectangular contact members of different widths [34, 35, 37, 38, 40, 41, 44]. The extension to an a-spot of arbitrary shape on a thin film was considered only in the limiting case of small film thickness [45, 46]. Though there have been recent studies to extend the modeling of electrical contacts to current conducting channels with linearly varying cross-sections [21], tunneling type contacts [32, 47, 48], and to AC conditions [49, 50], ideal and regular contact geometries are always assumed.

However, practically, due to the nature of contact edge roughness on a microscale, or due to the fabrication defects (e.g. misalignment of the contact edges), contact structures with irregular or tilted electrode edges are often formed (figure 1(a)). This is particularly common in microscale electrical contacts [51] and electrical contacts to two-dimensional (2D) materials, where a major challenge is patterning with very high precision [52]. Since the distribution of current flows near the electrical contact is highly sensitive to the conditions of the contact edge [45, 46], it is expected that the constriction resistance due to current crowding will be strongly affected by the irregularity of the contact shape. In addition, current flow through a rough constriction edge is often found in the electrical-potential-drop technique for measuring crack propagation in metal samples [53, 54]. The presence of inevitable edge roughness during crack propagation will introduce errors in the potential drop measurement (figure 1(b)). Hence, analyzing the current distribution and the constriction resistance in electrical contacts with irregular electrode edges is of great importance, which, however, is rarely treated in the literature.

In this paper, we study the spreading resistance and current crowding of rectangular electrical contacts with tilted contact edges (figure 2), using finite element method (FEM) based COMSOL simulations [55]. In section 2, the description of our model for a conducting contact structure with irregular

Table 1. Laplace equation and boundary conditions for the model in figure 2.

Inside CDEFGHIJ:	$\nabla^2\Phi = 0$
At HIJG:	$\Phi = 0$
At ABCD:	$\Phi = V_0$
At CDEF:	$\partial\Phi/\partial y = 0$
At ABHI, EFGJ:	$\partial\Phi/\partial z = 0$
At DEJI, CFGH:	$\partial\Phi/\partial x = 0$

electrode edge is given. Results and discussions are presented in section 3. The effects of contact edge tilt angle and contact electrode length are studied systematically. Summary and suggestions for future research are given in section 4.

2. Model description

In order to study the effects of irregular contact edges, we consider a simplified three-dimensional conducting structure with a tilted electrode edge, as shown in figure 2. The dimensions (a_1, a, a_2, b, h, W, θ) and the electrical resistivity (ρ) of the conductor are specified in figure 2. Current flows from the top electrode to the side electrode (cf. Figure 1(a)) when a bias voltage is applied between them. The length of the bulk conductor outside of the contact is $L_1 = b - a_1$ and $L_2 = b - a_2$ along the two sides, respectively, with an average length of $L = (L_1 + L_2)/2 = b - a$. In order to get the current flow profile and therefore the resistance of the structure in figure 2, we use a FEM based code, COMSOL [55], to solve the Laplace equation. The boundary conditions are summarized in table 1.

For the special case of $\theta = 0$, we have $a_1 = a_2 = a$ in the structure in figure 2. Here, due to symmetry, the width W can be ignored in solving the 2D Laplace equation (*i.e.* only in the y-z plane). This special case was studied by Hall [44] using conformal mapping calculation in the limit of $b \gg a$. The total resistance R_T between ABCD and HIJG with $\theta = 0$ for $b \gg a$ is found from Hall's exact calculation to be [37, 44],

$$R_T = R_{bulk} + R_s, \tag{1a}$$

$$R_{bulk} = \rho\frac{L}{hW}, \tag{1b}$$

$$R_s = \frac{\rho}{2\pi W}\overline{R_s}, \tag{1c}$$

$$\overline{R_s} = 2\pi\frac{a}{h} - 4\ln\left[\sinh\left(\frac{\pi}{2}\frac{a}{h}\right)\right], \tag{1d}$$

where $L = b - a$, R_{bulk} and R_s refer to the bulk resistance and the spreading resistance of the conducting structure, respectively, and all the symbols have been defined in figure 2. We have developed exact solutions for the potential profile $\Phi(x,y,z)$, for arbitrary values of dimensions a, b, h, W, and resistivity ρ, by using Fourier series expansion (cf. Eqs. (A1)—(A7) of [35]). From the exact field solution, we calculate the current density distribution, current flow patterns, and the resistance due to current crowding effects. It is verified that the Fourier series expansion method gives identical results to that of conformal mapping for $b \gg a$ [37]. When $a/h > 1$, it is also found that equation (1) is a very good approximation of the exact resistance for $L > h$ [35, 37, 41]. Numerical results from the FEM calculations will be verified against the exact theory (*i.e.* Equation (1)) for the special case of $\theta = 0$ in figure 2.

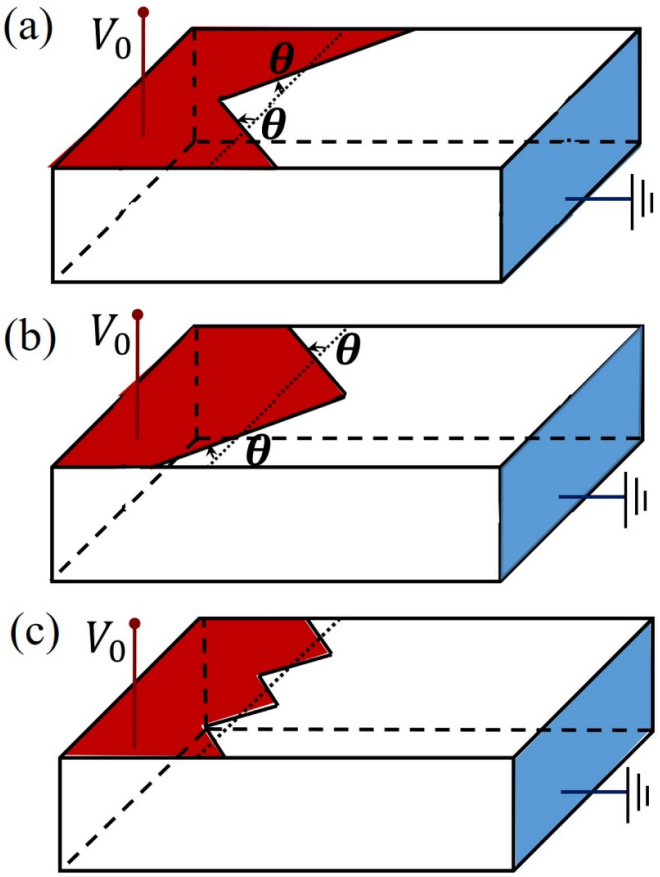

Figure 3. Irregular electrical contacts: (a), (b) with V-shaped contact edge, and (c) with saw-tooth contact edge.

It is noteworthy that, because of symmetry, the results in figure 2 can be directly extended to a V-shaped contact electrode edge, as shown in figures 3(a)–(b), which may be further generalized to a saw-tooth shaped contact edge in figure 3(c). The structure in figure 2 may be considered as a unit cell in characterizing the structures in figure 3.

3. Results

In this paper, we used the dimensions $b = 10$ cm, $h = 2$ cm, $W = 1$ cm, and assumed the resistivity $\rho = 1\Omega$m for all the cases calculated. Figure 4(a) shows the total resistance R_T of the structure in figure 2 as a function of the electrode length a for the special case of $\theta = 0$. As a decreases, R_T increases, this is because the current flow paths between the two electrodes become longer with decreasing a. The contributions from the

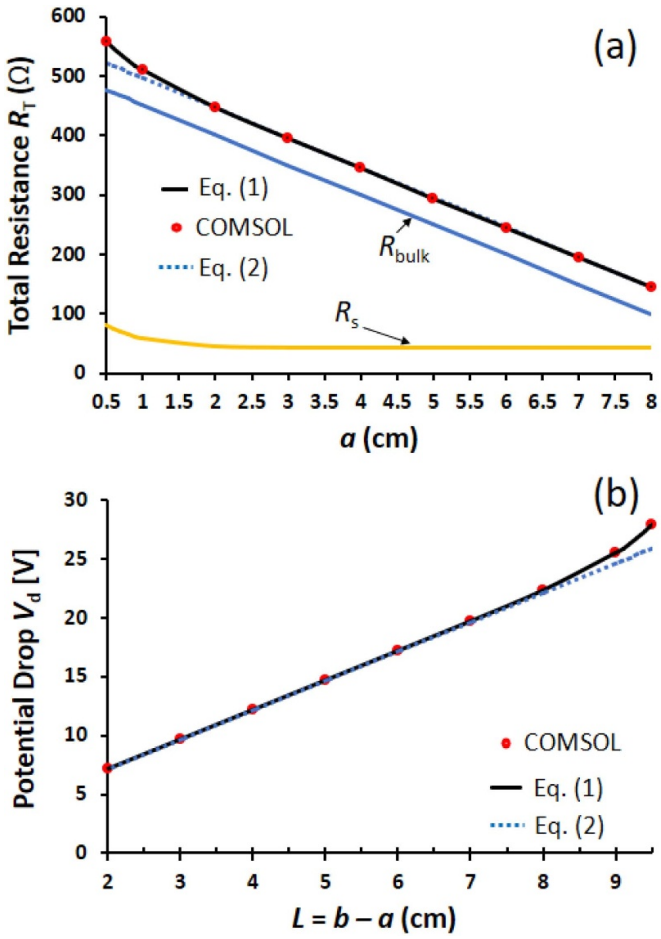

Figure 4. (a) Total resistance of the structure in figure 2 as a function of the electrode length a, for the special case of $\theta = 0$, (b) the corresponding voltage drop as a function of the length L when connecting to a contast current source $I_0 = 50$ mA. Symbols are for FEM simulation, solid lines are for theory from equation (1), and dotted lines are for linear approximations from equation (2). In (a), R_{bulk} and R_s calculated from equation 1 (b) and (c) respectively are also included.

bulk resistance R_{bulk} and the spreading resistance R_s, calculated from equations 1(b)–(c) respectively, are also shown in figure 4(a). It is clear that R_{bulk} decreases linearly with a, whereas R_s due to the current crowding effects decreases with a initially, and becomes almost a constant when $a > 2$ cm. When connecting to a constant current source I_0, the corresponding voltage drop V_d $(= R_T I_0)$ increases with the length L $(= b - a)$, as shown in figure 4(b). Excellent agreement between the FEM calculation and the theory of equation (1) are obtained, with a maximum error <0.004%. In the limit of $a \gg h$, we have [37] $\overline{R_s} = 4ln2$, which gives $R_s = \frac{\rho}{\pi W} 2ln2 = 0.441\ \rho/W$. Therefore, in the limit of $a \gg h$, the total resistance in equation (1) becomes,

$$R_T = (L/h + 0.441)\,\rho/W, \quad a \gg h \tag{2}$$

which is also plotted in figure 4(a). It is clear that the linear relation equation (2) gives a very good approximation to equation (1) when $a > h = 2$ cm. When $a < 2$ cm, the total resistance is increasingly larger than the linear prediction of equation (2). This is because when $a < h$, the intense current crowding effect near the constriction corner results in a higher spreading resistance R_s.

The effects of the angle of the electrode edge θ are shown in figures 5 and 6. Due to symmetry, the results for $+\theta$ and $-\theta$ are the same. As θ increases, the total resistance R_T, spreading resistance R_s, and the corresponding potential drop V_d all decrease, for a given electrode length a. For a given θ, the scalings with a in figures 5(a), (c)–(d) follow closely those of $\theta = 0$ in figure 2. It is important to note that for θ up to $\pm$ 60°, the change of the total resistance with respect to that at $\theta = 0$ is only < 14%, as shown in figures 5(b) and 6(a). This indicates that the total resistance R_T (and therefore the voltage drop V_d) for an irregular electrode edge with an average contact length of a (cf. Figure 2) can be estimated by using a rectangular electrode of $\theta = 0$ with the same contact length a, with an error < 14%, as long as the local angle θ is within $\pm$ 60°. For $\theta > 60°$, the total resistance can be reduced by $\sim 45\%$ (figure 5(b)). This is because the electrode length at the two sides for large θ (*i.e.* a_1 and a_2 in figure 2) can be very different from the average length (a in figure 2), yielding a very different current flow distribution, and thus a different resistance from the $\theta = 0$ case.

In contrast to the total resistance, the spreading resistance R_s depends strongly on the electrode angle θ, as shown in figures 5(c) and 6(b). This is because R_s is caused by the current crowding effect, which is sensitive to the local geometry near the constriction corners. For a given θ, the spreading resistance still decreases with the electrode length a, and eventually saturates for large a, as shown in figure 5(c). At $\theta = \pm 80°$, the spreading resistance R_s becomes negative for $a = 3$, 4, 5, 6, and 7 cm, as shown in figure 6(b). As already being pointed out in [37], the separation of the bulk resistance R_{bulk} and the spreading resistance R_s from the total resistance R_T, as defined in equations 1(c), is somewhat arbitrary, which is, however, adopted here by convention. The negative value of spreading resistance simply means the total resistance is smaller than 'bulk' resistance defined in equation 1(b). To further understand the behaviors of the resistance and current flow paths, we next present the current density distribution for various combination of electrode length a and electrode edge angle θ.

Figure 7 shows the current density in KNML, which is in the xz plane of the conducting structure shown in figure 2 and passes through the center of the tilted edge AB (cf. Figure 2.), for various θ. Note that, in the conducting structure shown in figure 2, current flows from the top electrode to the side electrode. For small θ (cf. Figure 7, $\theta = 5°$) the current density is almost uniformly distributed near KN. However, as θ increases the majority of the current density becomes concentrated near the center of KN (cf. Figure 7, $\theta = 80°$). The reason behind this is the fact that, in an electrical circuit, current always follows through the least resistive path and the maximum possible cross section area. For larger electrode edge angle, the current crowds near the constriction more strongly.

The current density distribution in the DCHI plane of the contact structure in figure 2 is shown in figure 8 for $\theta = 5°$, 10°, 30°, 45°, 60° and 80°, respectively. For small θ (cf. Figure 8, $\theta = 5°$) the current density is almost uniformly

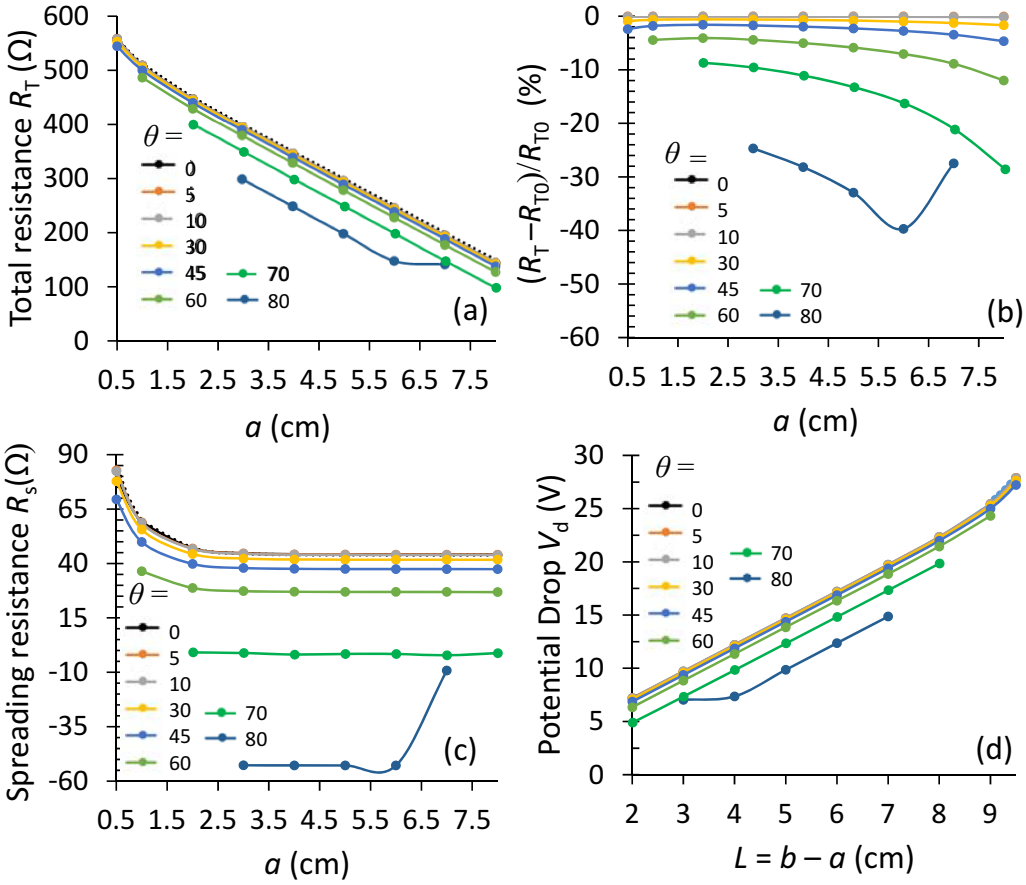

Figure 5. (a) Total resistance of the structure in figure 2, (b) the percentage change of the total resistance with respect to R_{T0}, the value at $\theta = 0$, (c) spreading resistance, and (d) the corresponding voltage drop when connecting to a contast current source $I_0 = 50$ mA, as a function of the electrode length a, for various θ. Symbols are for FEM simulation, lines between symbols for a guide for the eye. Dotted lines in (a) and (c) are from theoretical calculations using equation (1) for the special case of $\theta = 0$.

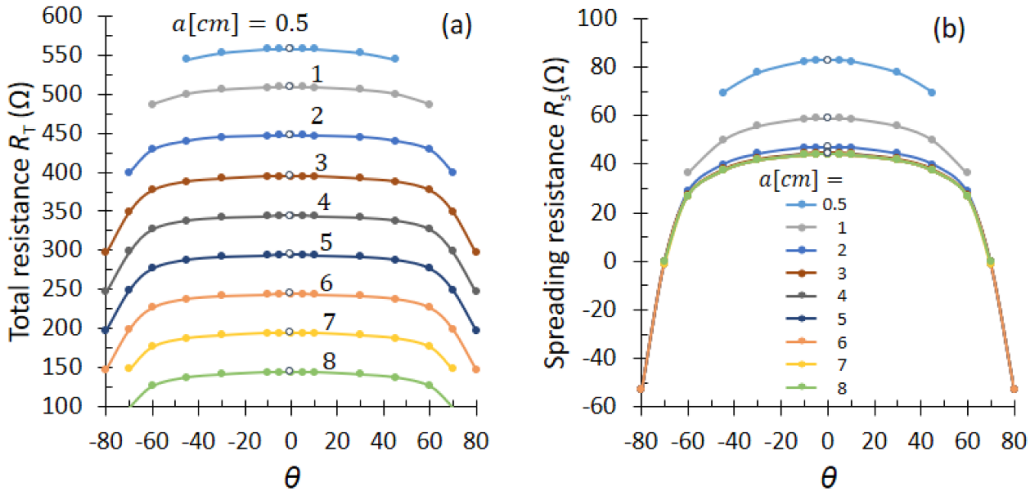

Figure 6. (a) Total resistance of the structure in figure 2, (b) the corresponding spreading resistance, as a function of θ, for different electrode length a. Symbols are for FEM simulation, lines between symbols for a guide for the eye. Open symbols are from theoretical calculations using equation (1) for the special case of $\theta = 0$.

distributed along the tilted edge AB. However, as θ increases, the majority of the current density tends to be concentrated near corner of the longer contact edge, point A (cf. Figure 8, $\theta = 80°$) due to the current crowding effect, which increases with the constriction in the structure. As a result, the current flow paths are significantly shortened for large θ, leading to a much reduced total resistance compared to the $\theta = 0$ case, as illustrated in figure 5 above.

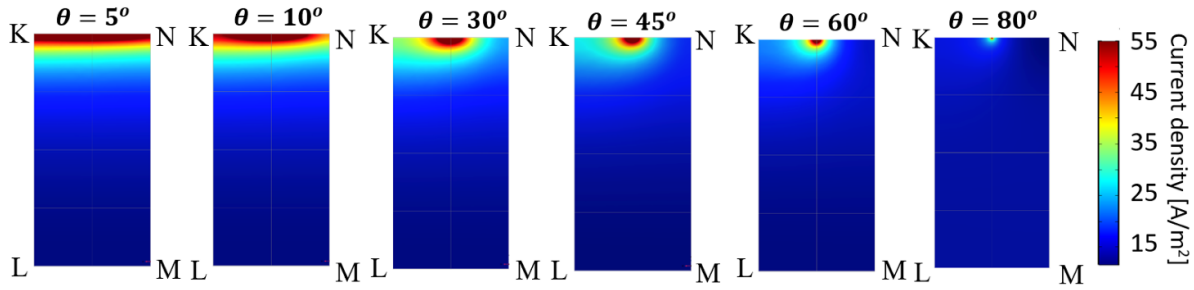

Figure 7. FEM simulation results for current density in KNML, which is in the *xz* plane (cf. figure 2) and passes through the center of the tilted edge (AB), for $\theta = 5^\circ,\ 10^\circ,\ 30^\circ,\ 45^\circ, 60^\circ$ and 80° respectively. The dimension and material properties of the conductor block are stated at the beginning of Section 3.

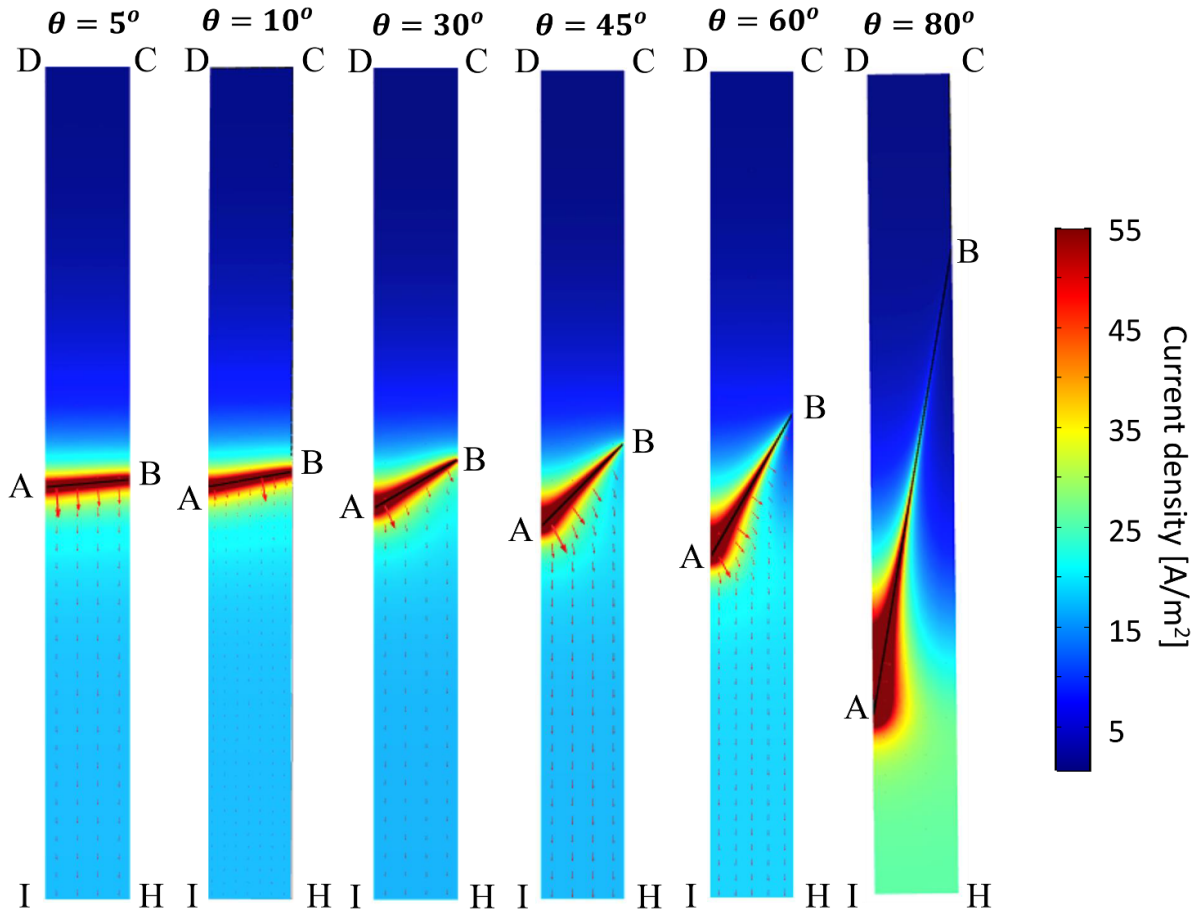

Figure 8. Current density in the DCHI plane of the structure shown in figure 2 for $\theta = 5^\circ,\ 10^\circ,\ 30^\circ,\ 45^\circ, 60^\circ$ and 80° respectively. The surface arrows represent the current flow direction. The dimension and material properties of the conductor block are stated in Section 3.

4. Summary

We have given a comprehensive analysis of the resistance and current distribution in a contact structure with irregular or tilted electrode edge, whose effects were typically ignored in previous studies. Using FEM calculations, the scaling of total resistance, spreading resistance, potential drop and current density distribution have been investigated for various electrode length a and electrode edge angle θ. For the special case of zero tilt angle, the results have been verified with the exact theory (equation (1)).

It is found that for a given electrode edge angle, both total resistance R_T and bulk resistance R_{bulk} decrease with electrode length a, for a given conductor length. However, the spreading resistance R_s decreases initially with a, and then becomes constant, following closely the scaling of the zero tilt angle case. As the contact edge angle θ increases, the spreading resistance and therefore the total resistance decreases. When $\theta < \pm 60^\circ$, the total resistance of the structure with tilted electrode edge in figure 2 with the chosen dimensions, can be estimated with an error $< 14\%$, by the simple structure with rectangular electrode ($\theta = 0^\circ$), which can be characterized using exact theory.

A detailed study of the current distribution shows nonhomogeneous distribution of the current density at the vicinity of the constriction and this nonuniformity increases with the electrode edge angle θ.

The conducting structure under study in figure 2 may be considered as the basic building block to better understand more complicated contact structures (e.g. Figure 3). Our study facilitates the strategic design of contact structures with controlled current distribution profiles and contact resistance. The results may also provide insights on interconnect and via resistance variation reduction in integrated circuit processing [56]. The effects of various contact geometry (circular, square, etc) and dissimilar materials may be studied in the future. Issues such as tunneling current [32, 47, 48], AC response [49, 50], and coupled electrical-thermal conduction [16, 28] in irregular electrical contacts may also be studied in the future.

The work is supported by the Air Force Office of Scientific Research (AFOSR) YIP Grant No. FA9550-18-1- 0061. The authors would like to thank Prof. Lalita Udpa and Prof. John Albrecht for useful discussions, and Mark Noto and Alex Olivero for assistance in COMSOL simulations.

ORCID iD

Peng Zhang https://orcid.org/0000-0003-0606-6855

References

[1] Holm R 1967 *Electric Contacts: Theory and Application* 4th edn (Berlin: Springer)
[2] Timsit R S 1999 Electrical contact resistance: properties of stationary interfaces *IEEE Trans. Compon. Packag. Technol.* **22** 85–98
[3] Slade P G 2017 *Electrical Contacts: Principles and Applications. Electrical and Computer Engineering* (Boca Raton, FL: CRC Press)
[4] Richter D, Adam J D, Depond J-M, Leroy D and Oberli L R 1997 DC measurement of electrical contacts between strands in superconducting cables for the LHC main magnets *IEEE Trans. Appl. Supercond.* **7** 786–92
[5] Booske J H 2008 Plasma physics and related challenges of millimeter-wave-to-terahertz and high power microwave generationa) *Phys. Plasmas 1994-Present* **15** 055502
[6] Gomez M R, Zier J C, Gilgenbach R M, French D M, Tang W and Lau Y Y 2008 Effect of soft metal gasket contacts on contact resistance, energy deposition, and plasma expansion profile in a wire array Z pinch *Rev. Sci. Instrum.* **79** 093512
[7] Manière C *et al* 2015 Pulse analysis and electric contact measurements in spark plasma sintering *Electr. Power Syst. Res.* **127** 307–13
[8] Hillairet J *et al* 2018 Radiofrequency and mechanical tests of silver coated CuCrZr contacts for the ITER ion cyclotron antenna *Fusion Eng. Des.* **129** 29–39
[9] Argouarch A *et al* 2014 RF contact development for the ITER ICRH antenna *AIP Conf. Proc.* **1580** 374–7
[10] Nijhuis A, Ilyin Y, Abbas W, Ten Haken B and Ten Kate H H J 2004 Change of interstrand contact resistance and coupling loss in various prototype ITER NbTi conductors with transverse loading in the twente cryogenic cable press up to 40,000 cycles *Cryogenics* **44** 319–39
[11] Calatroni S, Perret R and Vollenberg W 2006 RF contacts for the LHC collimators *Nucl. Instrum. Methods Phys. Res. Sect. Accel. Spectrometers Detect. Assoc. Equip.* **566** 205–11
[12] 2000 Review of federal programs for *wire system safety National Science and Technology Council Final Report*
[13] Kuzniar J S and Slenski G A 2001 Wire integrity field survey of USAF legacy aircraft *Report*ADP014075
[14] Haworth M D *et al* 1998 Significant pulse-lengthening in a multigigawatt magnetically insulated transmission line oscillator *IEEE Trans. Plasma Sci.* **26** 312–9
[15] Pedram M and Nazarian S 2006 Thermal modeling, analysis, and management in VLSI circuits: principles and methods *Proc. IEEE* **94** 1487–501
[16] Antoulinakis F, Chernin D, Zhang P and Lau Y Y 2016 Effects of temperature dependence of electrical and thermal conductivities on the Joule heating of a one dimensional conductor *J. Appl. Phys.* **120** 135105
[17] Allain A, Kang J, Banerjee K and Kis A 2015 Electrical contacts to two-dimensional semiconductors *Nat. Mater.* **14** 1195–205
[18] Datta S 2005 *Quantum Transport: Atom to Transistor* 2nd edition edn (Cambridge: Cambridge University Press)
[19] Lumbantobing A, Kogut L and Komvopoulos K 2004 Electrical contact resistance as a diagnostic tool for MEMS contact interfaces *J. Microelectromech. Syst.* **13** 977–87
[20] Almeida L, Ramadoss R, Jackson R, Ishikawa K and Yu Q 2006 Study of the electrical contact resistance of multi-contact MEMS relays fabricated using the MetalMUMPs process *J. Micromech. Microeng.* **16** 1189–94
[21] Zhang P, Gu Q, Lau Y Y and Fainman Y 2016 Constriction Resistance and current crowding in electrically pumped semiconductor nanolasers with the presence of undercut and Sidewall Tilt *IEEE J. Quantum Electron.* **52** 2000207
[22] Gu Q 2017 *Semiconductor Nanolasers* 1 edition edn (Cambridge: Cambridge University Press)
[23] Shiffler D, Zhou O, Bower C, LaCour M and Golby K 2004 A high-current, large-area, carbon nanotube cathode *IEEE Trans. Plasma Sci.* **32** 2152–4
[24] Tang W, Shiffler D, Golby K, LaCour M and Knowles T 2012 Experimental study of electric field screening by the proximity of two carbon fiber cathodes *J. Vac. Sci. Technol.* B **30** 061803
[25] Fairchild S B *et al* 2015 Morphology dependent field emission of acid-spun carbon nanotube fibers *Nanotechnology* **26** 105706
[26] Zhang P, Fairchild S B, Back T C and Luo Y 2017 Field emission from carbon nanotube fibers in varying anode-cathode gap with the consideration of contact resistance *AIP Advances* **7** 125203
[27] Fairchild S B *et al* 2019 Carbon nanotube fiber field emission array cathodes *IEEE Trans. Plasma Sci.* **47** 2032–8
[28] Zhang P *et al* 2018 Temperature comparison of looped and vertical carbon nanotube fibers during field emission *Appl. Sci.* **8** 1175
[29] Zhang P and Lau Y Y 2016 Ultrafast and nanoscale diodes *J. Plasma Phys.* **82** 595820505
[30] Zhang P, Valfells A, Ang L K, Luginsland J W and Lau Y Y 2017 100 years of the physics of diodes *Appl. Phys. Rev.* **4** 011304
[31] Lin J, Wong P Y, Yang P, Lau Y Y, Tang W and Zhang P 2017 Electric field distribution and current emission in a miniaturized geometrical diode *J. Appl. Phys.* **121** 244301
[32] Banerjee S, Luginsland J and Zhang P 2019 A two dimensional tunneling resistance transmission line model for nanoscale parallel electrical contacts *Sci. Rep.* **9** 14484
[33] Lau Y Y and Tang W 2009 A higher dimensional theory of electrical contact resistance *J. Appl. Phys.* **105** 124902

[34] Zhang P and Lau Y Y 2010 Scaling laws for electrical contact resistance with dissimilar materials *J. Appl. Phys.* **108** 044914
[35] Zhang P, Lau Y Y and Gilgenbach R M 2011 Thin film contact resistance with dissimilar materials *J. Appl. Phys.* **109** 124910
[36] Zhang P, Lau Y Y and Gilgenbach R M 2010 Minimization of thin film contact resistance *Appl. Phys. Lett.* **97** 204103
[37] Zhang P, Lau Y Y and Timsit R S 2012 On the spreading resistance of thin-film contacts *IEEE Trans. Electron Devices* **59** 1936–40
[38] Zhang P and Lau Y Y 2014 An exact field solution of contact resistance and comparison with the transmission line model *Appl. Phys. Lett.* **104** 204102
[39] Zhang P and Lau Y Y 2013 Constriction resistance and current crowding in vertical thin film contact *IEEE J. Electron Devices Soc.* **1** 83–90
[40] Zhang P, Hung D M H and Lau Y Y 2013 Current flow in a 3-terminal thin film contact with dissimilar materials and general geometric aspect ratios *J. Phys. D: Appl. Phys.* **46** 065502
[41] Zhang P, Lau Y Y and Gilgenbach R M 2015 Analysis of current crowding in thin film contacts from exact field solution *J. Phys. D: Appl. Phys.* **48** 475501
[42] Banerjee S, Wong P Y and Zhang P 2020 Contact resistance and current crowding in tunneling type circular nano-contacts *J. Phys. D: Appl. Phys.* **53** 355301
[43] Banerjee S, Cao L, Ang Y S, Ang L K and Zhang P 2020 Reducing contact resistance in two-dimensional-material-based electrical contacts by roughness engineering *Phys. Rev. Appl.* **13** 064021
[44] Hall P M 1968 Resistance calculations for thin film patterns *Thin Solid Films* **1** 277–95
[45] Zhang P 2015 Effects of surface roughness on electrical contact, RF heating and field enhancement *PhD Thesis* University of Michigan Ann Arbor (http://deepblue.lib.umich.edu/handle/2027.42/95929)
[46] Zhang P, Lau Y Y and Timsit R S Spreading resistance of a contact spot on a thin film *Holm Conf. on Electrical Contacts (HOLM), 2013 IEEE 59th Sep. 2013* pp 1–7
[47] Zhang P 2015 Scaling for quantum tunneling current in nano- and subnano-scale plasmonic junctions *Sci. Rep.* **5** 9826
[48] Banerjee S and Zhang P 2019 A generalized self-consistent model for quantum tunneling current in dissimilar metal-insulator-metal junction *AIP Advances* **9** 085302
[49] Timsit R S and Luttgen A 2016 Temperature distribution in an ohmic-heated electrical contact at high signal frequencies *Appl. Phys. Lett.* **108** 121603
[50] Antoulinakis F and Lau Y Y 2020 A theory of contact resistance under AC conditions *J. Appl. Phys.* **127** 125107
[51] Wang L *et al* 2019 Laser machined ultrathin microscale platinum thermometers on transparent oxide substrates *Sens. Actuators Phys.* **300** 111657
[52] Son J *et al* 2018 Atomically precise graphene etch stops for three dimensional integrated systems from two dimensional material heterostructures *Nat. Commun.* **9** 3988
[53] Horstman G and Lieb R 1979 Optimization of the electrical potential technique for crack growth monitoring in compact test pieces using finite element analysis *J. Test. Eval.* **7** 208–15
[54] Kuang W, Hesterberg J and Was G S 2019 The effect of post-irradiation annealing on the stress corrosion crack growth rate of neutron-irradiated 304L stainless steel in boiling water reactor environment *Corros. Sci.* **161** 108183
[55] COMSOL Multiphysics® Modeling Software (https://www.comsol.com/)
[56] Gu J, Zhao D, Kamon M, Fried D M, Harm G and Mountsier T, 2018 Electroless cobalt via pre-fill process for advanced BEOL metallization and via resistance variation reduction *2018 IEEE Int. Interconnect Technology Conf. (IITC)* pp 7–9